Atmos. Chem. Phys. Discuss., 15, 14889–14921, 2015
www.atmos-chem-phys-discuss.net/15/14889/2015/
doi:10.5194/acpd-15-14889-2015

Atmospheric Chemistry and Physics Discussions

Evaluation of regional background particulate matter concentration based on vertical distribution characteristics

S. Han[1,2], Y. Zhang[1], J. Wu[1], X. Zhang[1], Y. Tian[1], Y. Wang[1], J. Ding[1], W. Yan[1], X. Bi[1], G. Shi[1], Z. Cai[2], Q. Yao[2], H. Huang[2], and Y. Feng[1]

[1]State Environmental Protection Key Laboratory of Urban Ambient Air Particulate Matter Pollution Prevention and Control, College of Environmental Science and Engineering, Nankai University, Tianjin, 300071, China
[2]Research Institute of Meteorological Science, Tianjin, 300074, China

Received: 27 January 2015 – Accepted: 2 May 2015 – Published: 27 May 2015

Correspondence to: Y. Zhang (zhafox@126.com) and Y. Feng (fengyc@nankai.edu.cn)

Published by Copernicus Publications on behalf of the European Geosciences Union.

Abstract

Heavy regional particulate matter (PM) pollution in China has resulted in an important and urgent need for joint control actions among cities. It's advisable to improve the understanding of regional background concentration of PM for the development of efficient and effective joint control policies. With the increase of vertical height the influence of source emission on local air quality is weakening, but the characteristics of regional pollution gradually become obvious. A method to estimate regional background PM concentration is proposed in this paper, based on the vertical variation periodic characteristics of the atmospheric boundary layer structure and particle mass concentration, as well as the vertical distribution of particle size, chemical composition and pollution source apportionment. According to the method, the averaged regional background $PM_{2.5}$ concentration, being extracted from the original time series in Tianjin, was 40.0 ± 20.2, 63.6 ± 16.9 and $53.2 \pm 11.1\ \mu g\,m^{-3}$, respectively, in July, August and September.

1 Introduction

Atmospheric particulate matter (PM) has drawn considerable attention because it has been associated with many urban environmental problems, such as acid precipitation, decreasing visibility and climate change (Zeng and Hopke, 1989; Charlson et al., 1992; Schwartz et al., 1996; Chameides et al., 1999). PM has also been implicated in human mortality and morbidity (Dockery et al., 1993; Lagudu et al., 2011). Among the various sizes of atmospheric PM, $PM_{2.5}$ (PM with aerodynamic diameter less than 2.5 µm) is considered to be of great significance due to its links to human respiratory health (Englert, 2004) and regional-scale air pollution (Husar et al., 1981; Chameides et al., 1999).

With rapid industrialization and urbanization, high PM concentration level is considered to be one of the most serious pollution problems in China (Tie et al., 2006; Liu

ACPD
15, 14889–14921, 2015

et al., 2011; Chen et al., 2012; Han et al., 2013). In addition, regional compound pollution, such as haze and acid precipitation, has become a prominent problem. The origin of PM is complex. It involves both initial emissions as well as secondary chemical reactions (Shi et al., 2011; Tian et al., 2013; Hu et al., 2013; Guo et al., 2013). With a lifetime of days to weeks in the lower atmosphere, $PM_{2.5}$ can be transported thousands of kilometers (Hagler et al., 2006). The trans-boundary transport and transform of $PM_{2.5}$ and the gaseous precursors may result in air pollution associated with each other among cities, which has significant influence on the regional background PM level in the city cluster. In order to study the regional-scale PM pollution and develop efficient joint control policies, it's necessary to improve understanding of regional background PM concentration.

Background concentration has been defined as concentration observed at a site "that is not affected by local sources of pollution" (WHO, 1980; Menichini et al., 2007). McKendry (2006) defined background concentration as one of "those pollutants arising from local natural processes together with those transported into an airshed from afar (the latter may be either natural or anthropogenic in origin)". Background concentration in this paper is defined to include collective contributions from regional anthropogenic and natural emissions and long-range transport.

Background concentrations are not constant because of meteorological variability, complexity of chemical reactions, as well as spatially and temporally varying emissions. Regional-scale PM pollution is associated with synoptic scenarios that induce the transfer, accumulation and the formation of pollutants at regional scales (Ronald et al., 2007). Simply taking measurements at local scales is not well suited to adequately investigate the regional background concentration. There is always the possibility that the "air quality background monitoring station" is directly influenced by local emission sources and thus not truly representative of the background level (Tchepel et al., 2010). That is to say, background concentration can hardly be measured directly, so it is critical to choose representative and appropriate values. Usually, by setting some restrictions to identify and remove the influence of local pollution, background

ACPD
15, 14889–14921, 2015

concentration can be determined indirectly. There are several studies mentioning the methods for determining the background concentration. These methods can be classified into 4 categories. (1) The physical methods identify the regional pollution process and local pollution process via the synoptic situation, duration of the synoptic system, consistency of vertical wind, and atmospheric stability etc., and then the data of the "background period" which are influenced by regional processes are selected (Pérez et al., 2008). (2) The chemical methods identify the regional process according to the size distribution or chemical composition of the PM and synchronous observation of other pollutants, and then remove the data influenced by local processes (Menichini, 2007). (3) The statistical methods use discriminant analysis, cluster analysis and principal component analysis (PCA) to identify the data that characterize the regional background PM (Langford et al., 2009; Tchepel et al., 2010). (4) Numerical simulation methods use trajectory models and atmospheric dynamics-chemical coupled models to simulate the regional background pollution (Dreyer et al., 2009; Tchepel et al., 2010).

With the increase of vertical height, the influence of source emission on local air quality is weakening, but the characteristics of regional pollution gradually become obvious. Influenced by atmospheric dynamics and thermal effects, meteorological variables and pollutant measurements at different heights within the boundary layer could represent different horizontal scales of pollution. Sites at near ground height (5–10 m) are influenced extensively by human activities, and the data observed at these sites could represent the street scale. Impacts from local disturbance weakening with height gradually and observations at greater heights could represent larger horizontal scales. When the height increases to the top of the urban atmospheric boundary layer, observations can represent urban scales. Heights above the urban boundary layer could to some extent reflect the characteristics of regional scales. Gradient observations of meteorological variables and ultrasonic anemometer observations can be used to analyze vertical variations of local diffusion conditions. The height influenced relatively less by local pollution emission can be determined and then the regional background PM concentration can be extracted from the observation data by mathematical methods.

ACPD
15, 14889–14921, 2015

In this paper, the periodic variation of the atmospheric boundary layer structure and vertical particle mass concentrations, as well as the vertical distribution characteristics of particle size, chemical composition and pollution sources were studied to provide scientific basis for characterizing the regional pollution contribution and to evaluate regional background PM concentration levels.

2 Data sources and treatment

2.1 Observation site

The data used in this study were collected at a 255 m meteorological tower which is located at the atmospheric boundary layer observation station (39°04′29.4″ N, 117°12′20.1″ E) in Tianjin, China, where is a residential and traffic mixing area. There are no industrial pollution sources near the site. Tianjin is adjacent to the BoHai Sea and situated in the eastern part of the Beijing–Tianjin–Hebei area, one of the most heavily polluted areas in China. Tianjin covers an area of 11 300 km^2 and has a population of 8 million. Due to rapid industrialization and urbanization in recent years, air pollution has become a serious problem in this city.

2.2 Observation method and data treatment

Horizontal wind speed, wind direction, and temperature were measured at 15 platforms (5, 10, 20, 30, 40, 60, 80, 100, 120, 140, 160, 180, 200, 220 and 250 m) every 10 s and averaged hourly. Three dimensional ultrasonic anemometers (CAST-3D) were mounted at 40, 120 and 220 m to measure the turbulent fluxes. Hourly meteorological data in the year of 2009 were used in this paper.

Hourly averaged mass concentrations of $PM_{2.5}$ were measured at four levels (2, 40, 120, and 220 m) by ambient particulate monitor chemiluminescence (TEOMR-RP1400a) in autumn, 2009.

ACPD
15, 14889–14921, 2015

In order to study the vertical characteristics of PM chemical compositions and sources, PM_{10} samples were collected at the heights of 10, 40, 120, and 220 m from 24 August to 12 September 2009. At each height, PM_{10} samples were collected using two samplers in parallel: one is for chemical analysis of inorganic composition on polypropylene filters (90 mm in diameter, Beijing Synthetic Fiber Research Institute, China) and the other is for organic composition analyses on quartz-fiber filters (90 mm in diameter, 2500QAT-UP, Pall Life Sciences). All samples were collected in a 24 h period every day and at a flow rate of 100 L min^{-1}. Elements (Si, Ti, Al, Mn, Ca, Mg, Na, K, Cu, Zn, As, Pb, Cr, Ni, Co, Cd, Hg, Fe and V) were analyzed by Inductively Coupled Plasma-atomic emission spectroscopy (ICP 9000(N + M)Thermo Electron Corporation, USA). Water-soluble ions (Na^+, K^+, Ca^{2+}, Mg^{2+}, NH_4^+, NO_3^- and SO_4^{2-}) were analyzed by ion chromatography (DX-120, Dionex Ltd., USA) after extraction by deionized water. The thermal optical carbon analyzer (Desert Research Institute (DRI) Model 2001, Atmoslytic Inc., Calabasas, CA, USA) was used to measure organic carbon (OC) and elemental carbon (EC).

3 Vertical variation characteristics of urban boundary structure

3.1 Thermal and dynamic characteristics in near surface layer

Surface layer is closely related to the diffusion of air pollutants. This layer is strongly affected by the human behavior on the ground. Figure 1 shows diurnal variation of averaged wind speed in four seasons at different heights in Tianjin. Similar change rules were in effect in each season. The wind speed is high in daytime and low at night below 100 m, while, low wind speed in daytime and high at night above 100 m.

The vertical distribution profile of wind speed and temperature under different stability are shown in Fig. 2. The temperature profile correlates weakly with height over 100 m and the wind speed profile correlates weakly with height over 150 m. The atmospheric layer at 100–160 m is considered as a special stratification, the variation rules

ACPD
15, 14889–14921, 2015

of temperature and wind speed with height were different compared with the upper and lower layers.

3.2 The height of nocturnal planetary boundary and vertical variation of turbulent intensity

The height of the planetary boundary layer (PBL), indicating the range of pollutants diffused by thermal turbulence in the vertical direction (Kim et al., 2007; Lena and Desiato, 1999), can be calculated by wind and temperature profiles (Seibert et al., 2000; Han et al., 2009). In this paper, temperature gradient data observed at the tower were used to analyze the nocturnal planetary boundary layer height (NPBL) in different seasons (Fig. 3). The seasonal variation of the NPBL height is generally small, with seasonal averaged NPBL height ranging from 114 to 142 m.

In this paper, hourly averaged mass concentrations of $PM_{2.5}$ and PM_{10} were measured at four platforms (2, 40, 120, and 220 m). The heights of the 1st and 2nd platform are inside the NPBL, the 3rd platform is located at the top of the NPBL and the 4th platform is generally outside the NPBL. Due to the dynamical stability of the NPBL, air pollutants in surface layer are normally trapped inside the NPBL and rarely mix with the pollutants outside the NPBL. Very different distribution characterizations of PM were measured inside and outside the NPBL (see Sect. 4).

Based on the observation data from the three dimensional ultrasonic anemometers, the turbulent intensity were calculated. Averaged diurnal variation of turbulent intensity at different heights is shown in Fig. 4. Three dimensional components of turbulent intensity decreased with increase in height. From the height of 40 to 120 m, the u, v and w components of turbulent intensity reduced by 27, 32 and 21 %, respectively. From 120 to 220 m, the u, v and w components reduced by 12, 13 and 15 %, respectively. The descending trend is more obvious from 40 to 120 m than that of from 120 to 220 m.

ACPD
15, 14889–14921, 2015

4 Vertical distribution of $PM_{2.5}$ mass concentration

The vertical variation of $PM_{2.5}$ mass concentrations is shown in Fig. 5. Among these 4 platforms (2, 40, 120 and 220 m), $PM_{2.5}$ concentration at 220 m at night is the lowest. The NPBL height generally ranges from 100 to 150 m in Tianjin, and the height of 220 m is just outside the NPBL. This indicates that the observation value of 220 m at night is less affected by local sources of emission and is largely attributed to regional scale pollution.

At night, the pollutants emitted from the surface diffuse upwards and accumulate in the NPBL. This leads to the highest concentration of $PM_{2.5}$ at the height of 120 m, which is near the top of the NPBL. After sunrise, the inversion layer is gradually destroyed, pollutants near the ground gradually diffuse upward and the $PM_{2.5}$ concentration near the surface gradually decreases. At the height of 120 and 220 m, the peak of pollutant concentration appears at approximately 08:00 and 09:00 LT respectively. At noontime, the mixing layer is fully developed and three observation levels are all inside the PBL.

5 Vertical distributions of PM_{10} concentration, components and source apportionment

5.1 Vertical characteristics of PM_{10} concentration

As mentioned in Sect. 2.2, PM_{10} samples were collected at the heights of 10, 40, 120 and 220 m. The daily concentrations at each sampling height were 139 ± 45, 121 ± 43, 110 ± 39 and $79 \pm 37\ \mu g\,m^{-3}$, respectively. These concentrations exhibited a general decreasing trend with the increase of height.

The height-to-height correlation coefficients of the variation of PM_{10} concentration were calculated and listed in Table 1. All the pairwise correlation coefficients among 10, 40 and 120 m were higher than 0.9. However, the correlation coefficients between 220 m and other heights were obviously low. These results suggest that the influences

ACPD
15, 14889–14921, 2015

of local emissions and local meteorological diffusion conditions on PM_{10} concentrations are weaker at 220 m than that at lower levels.

5.2 Vertical characteristics of PM_{10} chemical components

Nineteen elements were analyzed from PM_{10} samples collected at four heights. In order to study the vertical variations of element profiles at the four heights, coefficients of divergence (CD) (Wongphatarakul et al., 1998; Hwang et al., 2008) were used. CD can be calculated as following:

$$CD_{jk} = \sqrt{\frac{1}{p}\sum_{i=1}^{p}\left(\frac{x_{ij}-x_{ik}}{x_{ij}+x_{ik}}\right)^2} \quad (1)$$

where, x_{ij} is the average concentration of the ith element at jth height. j and k represent the two sampling heights, and p is the number of elements. When the species concentrations at two sampling sites were similar to each other, the CD values would approach 0. On the other hand, as the two species concentrations diverge, the CD value will approach 1 (Hwang et al., 2008).

The pair-wise CD values for four heights are shown in Table 2. The pair-wise CD values among 10, 40 and 120 m are lower than 0.2, illustrating that the element profiles of these three heights were similar to each other. While, the CD values between 220 m and the other three levels were obviously high, indicating a larger difference in element profiles. This may be resulted from the elements of the PM_{10} samples at 220 m were mainly originated from regional-scale sources.

The concentration of chemical components of ambient PM_{10} samples collected at 4 heights are shown in Table 3. Al, Si, Ca, OC, EC, Cl^-, NO_3^- and SO_4^{2-} have higher concentration levels than other species. Al can be used as a source marker of coal combustion (Hopke, 1985); Al and Si are the markers of soil dust (Liu et al., 2003), Ca is mainly emitted from cement dust (Shi et al., 2009); EC can be identified as vehicle exhaust emission (Li et al., 2004); Cl^- is the marker for sea salt (Li et al.,

ACPD
15, 14889–14921, 2015

2004); and NO_3^- and SO_4^{2-} are the markers of secondary nitrate and sulfate (Liu et al., 2003). Higher concentrations were found at lower sampling sites for almost all species (NO_3^- had the highest value at 120 m). Unlike the species concentration, the vertical distribution of species percentages (%) shows different patterns. Similar fraction levels were observed at the four heights for Al and Si. For Ca and EC, higher values were observed at lower sampling sites. The percentages of OC at 220 m were obviously higher than those at 120 m. This might imply that the influence of local sources on OC was weaker and the contributions from secondary and regional sources were larger at 220 m. The OC/EC ratios increased gradually from 10 to 220 m. This might be due to a relatively higher percentage of SOC in OC at higher heights as results of the formation and regional transport of SOC (Strader et al., 1999). Similarly, the higher sampling sites obtained higher fractions (%) for NO_3^- and SO_4^{2-} (the highest percentage of NO_3^- were observed at 120 m). These trends suggest that the impact of primary sources from the ground decreased with the increase of height, while the impact of secondary sources mainly influenced by regional sources becomes more prominent.

5.3 Vertical characteristics of PM_{10} sources

In order to understand the vertical characteristics of PM_{10} sources, the chemical mass balance (CMB) model was applied for source apportionment at all four heights. The CMB model, a useful receptor model, has been extensively used to estimate source categories and contributions to the receptor based on the balance between sources and the receptor (Chow et al., 2007; Watson et al., 2008). Further details of CMB can be found in the literature (Watson et al., 1984, 2002; USEPA, 2004).

Seven source categories (coal combustion, crustal dust, cement dust, vehicle exhaust, sea salt, secondary sulfate and secondary nitrate) and their source contributions ($\mu g\,m^{-3}$) and percentage contributions (%) estimated by the CMB model are listed in Table 4. The estimated source contributions ($\mu g\,m^{-3}$) of all the sources showed a downward trend with the increase of height. While the percentage contributions (%) of sec-

ACPD
15, 14889–14921, 2015

ondary sources (secondary sulfate and nitrate) presented a generally upward trend with the increase in height. This might be due to the fact that for the secondary sources the particulate sizes are relatively smaller and the residence time of fine particle is longer. Generally, secondary sources can obtain stronger influence from regional contributions (Gu et al., 2011). That is to say, PM at higher heights obtain more regional contributions. And, to some extent, this could reflect the characteristics at the regional scale.

6 Vertical variation of periodicity for the time series of $PM_{2.5}$ concentrations and meteorological variables

The periodic characteristics of particulate concentration and meteorological variables can reflect different scales of atmospheric processes. In this paper, the vertical variation period of the atmospheric boundary layer variables and particle mass concentrations were analyzed.

Time series of atmospheric pollutant concentration and relative meteorological variables could be decomposed into baseline and short-term components. Using the filtering method, short-term fluctuations associated with the influence of local-scale pollution and dispersion conditions can be extracted from the original measurements. After the removal of local-scale effects, the time series of pollutant concentrations can be reconstructed to reflect the regional scale influence.

6.1 Filtering method

The wavelet transform can be used to analyze time series that contain nonstationary signals at many different frequencies. In this paper, we chose the Morlet wavelet which is extensively used in studies of climate change and turbulence power spectrum analysis (Torrence and Compo, 1998). The normalization mother wavelet is shown in

ACPD
15, 14889–14921, 2015

Eq. (2).

$$\psi_0(\eta) = \pi^{-1/4} e^{i\omega_0 \eta} e^{-\eta^2/2} \tag{2}$$

where η is the nondimensional time parameter and ω_0 is the nondimensional frequency. The wavelet filter time series over a set of scales can be calculated by:

$$x_n = \frac{\delta j \delta t^{1/2}}{C_\delta \psi_0(0)} \sum_{j=0}^{J} \frac{R\{W_n(s_j)\}}{s_j^{1/2}} \tag{3}$$

where δj is the spacing between the discrete scales, and δt is the sampling interval. S_j is a set of scales related to the frequency ω. C_δ and $\psi_0(0)$ are both constants.

$$\omega = \frac{\omega_0 + \sqrt{2 + \omega_0^2}}{4\pi s} \tag{4}$$

The reconstruction then gives:

$$C_\delta = \frac{\delta j \delta t^{1/2}}{\psi_0(0)} \sum_{j=0}^{J} \frac{R\{W_\delta(s_j)\}}{s_j^{1/2}} \tag{5}$$

According to the conservation of total energy under the wavelet transform and the equivalent of Parseval's theorem for wavelet analysis, the variance of the time series is:

$$\sigma^2 = \frac{\delta j \delta t}{C_\delta N} \sum_{n=0}^{N-1} \sum_{j=0}^{J} \frac{\left|W_n(s_j)\right|^2}{s_j} \tag{6}$$

Both Eqs. (5) and (6) should be used to check wavelet routines for accuracy and to ensure that sufficiently small values of s_0 and δj have been chosen. The values of the above parameters are given in Table 5.

ACPD
15, 14889–14921, 2015

As discussed above, the wavelet transform is essentially a bandpass filter. By summing over a subset of the scales in Eq. (3), a wavelet-filtered time series can be constructed as follows:

$$x_n' = \frac{\delta j \delta t^{1/2}}{C_\delta \psi_0(0)} \sum_{j=j_1}^{j_2} \frac{R\{W_n(s_j)\}}{s_j^{1/2}} \quad (7)$$

This filter has a response function given by the sum of the wavelet functions between scale j_1 and j_2.

6.2 Fluctuation spectrum analysis of $PM_{2.5}$ concentration time series at different heights

The fluctuation spectrum distribution of hourly mass concentrations of $PM_{2.5}$ on the ground and at the height of 2, 40, 120 and 220 m were analyzed in this paper. The missing data in the time series was computed by interpolation. Because of low proportions and unconcentrated distributions in the missing data, little human interference was brought to the spectral composition of the original time series. For better comparison, normalization (standard variance 1, mean 0) of the original time series was necessary prior to power spectrum analysis.

The local and global wavelet power spectrum contours for the time series of $PM_{2.5}$ concentrations at different heights in August are shown in Fig. 6. Contours are expressed as $\log_2(|W_n(s)|^2)$ because of large magnitudes. Area inside the thick black solid line passes the red noise standard spectral test with the 5 % significance level. Area outside the blue dotted line was excluded from analysis because of poor reliability from the cone of influence, where edge effects become important. The global wavelet spectrum $\overline{W^2}(s)$, which reflects characteristics of the pollutant concentration time series in the frequency domain, was obtained by calculating the average of local wavelet spectrums $|W_n(s)|^2$ over the entire sampling time domain. The solid line is the global

ACPD
15, 14889–14921, 2015

wave spectrum for the corresponding time series. The dashed line is the 5 % significance level, the upper area of which passes the red noise standard spectral test at the 5 % significance level.

The global wavelet power spectrum of $PM_{2.5}$ mass concentration shows that fluctuations of 6–10 days (related to weather process and regional-scale pollution) are significant at each observation height, while fluctuations of 12–24 h (mainly concerned with the daily variation of atmospheric boundary layer and local pollution emissions by human activities) are significant only on ground level. For the fluctuations of $PM_{2.5}$ mass concentration, wave energy of 6–10 days period reduces with the increase of height. In terms of the local power spectrum, 12–24 h period can be observed in a few days on the ground. But with the increase of height, the power of 12–24 h period became weaker, only 10–30 % of that on the ground.

7 Determination of regional background concentration of particulate matter

According to the above research concerning the vertical distribution characteristics of particle size, chemical composition and pollution sources, as well as the fluctuation power spectrum analysis of the atmospheric boundary layer structure and particle mass concentration, the nocturnal $PM_{2.5}$ mass concentration time series with the 6–10 days period at the height of 220 m were extracted to characterize the regional background concentration, which mainly associated with the regional scale pollution.

Due to short-term fluctuations of pollution emission and local diffusion conditions, observation errors, and etc., the original $PM_{2.5}$ concentration time series presents violent oscillation. Using wavelet transformation, the nocturnal $PM_{2.5}$ mass concentration time series with the 6–10 days period at the height of 220 m was extracted from the original time series. After the filtering, impacts from local-scale pollution and diffusion conditions on the short-term fluctuations have been removed. Thus regional-scale pollution and synoptic-scale weather conditions were better represented in the remaining part (shown in Fig. 7).

ACPD
15, 14889–14921, 2015

According to the method proposed in this paper, in Tianjin, the averaged regional background $PM_{2.5}$ concentrations in July, August and September 2009 were 40.0 ± 20.2, 63.6 ± 16.9 and 53.2 ± 11.1 μg m^{-3}, respectively.

8 Summary and conclusions

It is crucial for studying regional-scale PM pollution and for the development of efficient joint control policy to improve understanding of the regional background concentration of PM. Based on the spectrum analysis of vertical variation of the atmospheric boundary layer structure and particle mass concentration, as well as the vertical distribution of particle size, chemical composition and pollution source apportionment, a method to estimate regional background PM concentration is proposed in this paper.

Based on a 255 m meteorological tower, the vertical thermodynamic and dynamic characteristics of the atmospheric boundary layer in Tianjin was observed. The atmospheric layer at 100–160 m was considered as a special stratification, the variation rules of temperature and wind speed with height were different in comparing with upper and lower layers. The turbulent intensity decreased with increase in height and the descending trend is more obvious from 40 to 120 m than that of from 120 to 220 m. Seasonal averaged nocturnal planetary boundary layer height ranges from 100 to 150 m. The observation height of 220 m is just outside the NPBL, which indicates that the observation value of PM concentration at 220 m at night is less affected by local primary sources near the ground and is largely contributed by regional scale pollution.

The vertical distribution of chemical components in PM_{10} samples also suggests that the impact of primary sources near the ground decreased with the increase in height, while the impact of secondary sources mainly influenced by regional sources became more prominent. The vertical distribution of percentage was different for various species. Similar percentage levels were observed at the four different heights for Al and Si. For the Ca and EC fractions, higher values were observed at lower sampling sites. The percentages of NO_3^-, SO_4^{2-} and OC, and the OC/EC ratios were obviously

ACPD
15, 14889–14921, 2015

higher at higher sites. Source apportionment for ambient PM_{10} showed that the percentage contributions of secondary sources obviously increased with height, while the contribution of cement dust decreased with height. PM at higher height obtained more regional contributions, and to some extent, it could reflect the characteristics of the regional scale.

The periodic characteristics of $PM_{2.5}$ mass concentration can reflect different scales of atmospheric processes. In terms of global wavelet power spectrum of $PM_{2.5}$ mass concentration, fluctuations of 6–10 days, related to weather processes and regional-scale pollution, were significant at each observation height. While fluctuations of 12–24 h, mainly concerned with the daily variation of atmospheric boundary layer and local pollution emissions by human activities in the surface layer, were significant only on ground level. In terms of the local power spectrum, 12–24 h period can be observed in a few days on the ground. But with the increase of height, the power of 12–24 h period became weaker, only 10–30 % of that on the ground.

According to the above research, the nocturnal $PM_{2.5}$ mass concentration time series with the 6–10 days period at the height of 220 m can be regarded as regional background concentration, which mainly associated with the regional scale pollution. Using wavelet transformation and filtering, the nocturnal $PM_{2.5}$ mass concentration time series with the 6–10 days period at the height of 220 m was extracted from the original time series. After removing the impacts from local-scale pollution and diffusion conditions on the short-term fluctuations, regional-scale pollution and synoptic-scale weather conditions were better represented in the remaining part. According to the method proposed in this paper, in Tianjin, the averaged regional background $PM_{2.5}$ concentrations in July, August and September 2009 were 40.0 ± 20.2, 63.6 ± 16.9 and $53.2 \pm 11.1\ \mu g\,m^{-3}$, respectively.

We attempted to put forward a new method to estimate the regional background concentration of PM. Background PM concentrations are not constant but varying with space and time. In future research, more analysis on the characteristics of the urban boundary layer, vertical distribution of PM components and source apportionment in

ACPD
15, 14889–14921, 2015

different seasons and meteorological conditions will be done, and background concentration ranges of $PM_{2.5}$ for given time periods and meteorological conditions will be obtained.

Acknowledgements. This work was funded by the Tianjin science and technology projects (14JCYBJC22200), the Science and Technology Support Program(13ZCZDSF02100), and the National Natural Science Foundation of China (NSFC) under Grant No.41205089 and No.21207069. We also thank LetPub (www.letpub.com) for its linguistic assistance during the preparation of this manuscript.

References

Chameides, W. L., Yu, H., Liu, S. C., Bergin, M., Zhou, X., Mearns, L., Wang, G., Kiang, C. S., Saylor, R. D., and Luo, C.: Case study of the effects of atmospheric aerosols and regional haze on agriculture: an opportunity to enhance crop yields in China through emission controls, P. Natl. Acad. Sci. USA, 96, 13626–13633, 1999.

Charlson, R. J., Schwartz, S. E., Hales, J. M., Cess, R. D., Coakley, J. A., Hansen, J. E., and Hofmann, D. J.: Climate forcing by anthropogenic aerosols, Science, 255, 423–430, 1992.

Chow, J. C., Watson, J. G., Lowenthal, D. H., Chen, L. W. A., Zielinska, B., Mazzoleni, L. R., and Magliano, K. L.: Evaluation of organic markers for chemical mass balance source apportionment at the Fresno Supersite, Atmos. Chem. Phys., 7, 1741–1754, doi:10.5194/acp-7-1741-2007, 2007.

Chen, J., Zhao, C. S., Ma, N., Liu, P. F., Göbel, T., Hallbauer, E., Deng, Z. Z., Ran, L., Xu, W. Y., Liang, Z., Liu, H. J., Yan, P., Zhou, X. J., and Wiedensohler, A.: A parameterization of low visibilities for hazy days in the North China Plain, Atmos. Chem. Phys., 12, 4935–4950, doi:10.5194/acp-12-4935-2012, 2012.

Dockery, D. W., Pope, C. A., Xu, X., Spengler, J. D., Ware, J. H., Fay, M. E., Ferris Jr., B. G., and Speizer, F. E.: An association between air pollution and mortality in 6 United States cities, N. Engl. J. Med., 329, 1753–1759, 1993.

Dreyer, A. and Ebinghaus, R.: Poly fluorinated compounds in ambient air from ship- and land-based measurements in northern Germany, Atmos. Environ., 43, 1527–1535, 2009.

Englert, N.: Fine particles and human health-a review of epidemiological studies, Toxicol. Lett., 49, 235–242, 2004.

ACPD
15, 14889–14921, 2015

Gu, J. X., Bai, Z. P., Li, W. F., Wu, L. P., Liu, A. X., Dong, H. Y., and Xie, Y. Y.: Chemical composition of $PM_{2.5}$ during winter in Tianjin, China, Particuology, 9, 215–221, 2011.
Guo, S., Hu, M., Guo, Q., Zhang, X., Schauer, J. J., and Zhang, R.: Quantitative evaluation of emission controls on primary and secondary organic aerosol sources during Beijing 2008 Olympics, Atmos. Chem. Phys., 13, 8303–8314, doi:10.5194/acp-13-8303-2013, 2013.
Hagler, G. S. W., Bergin, M. H., Salmon, L. G., Yu, J. Z., Wan, E. C. H., Zheng, M., Zeng, L. M., Kiang, C. S., Zhang, Y. H., Lau, A. K. H., and Schauer, J. J.: Source areas and chemical composition of fine particulate matter in the Pearl River Delta region of China, Atmos. Environ., 40, 3802–3815, 2006.
Han, S. Q., Bian, H., Tie, X. X., Xie, Y. Y., Sun, M. L., and Liu, A. X.: Impact of nocturnal planetary boundary layer on air pollutants: measurements from a 250 m tower over Tianjin, China, J. Hazard. Mater., 162, 264–269, 2009.
Han, X., Zhang, M. G., Tao, J. H., Wang, L. L., Gao, J., Wang, S. L., and Chai, F. H.: Modeling aerosol impacts on atmospheric visibility in Beijing with RAMS-CMAQ, Atmos. Environ., 72, 177–191, 2013.
Hu, W. W., Hu, M., Yuan, B., Jimenez, J. L., Tang, Q., Peng, J. F., Hu, W., Shao, M., Wang, M., Zeng, L. M., Wu, Y. S., Gong, Z. H., Huang, X. F., and He, L. Y.: Insights on organic aerosol aging and the influence of coal combustion at a regional receptor site of central eastern China, Atmos. Chem. Phys., 13, 10095–10112, doi:10.5194/acp-13-10095-2013, 2013.
Husar, R. B., Holloway, J. M., Patterson, D. E., and Wilson, W. E.: Source areas and chemical composition of fine particulate matter in the Pearl River Delta region of China, Atmos. Environ., 15, 1919–1928, 1981.
Hopke, P. K.: Indoor air pollution: radioactivity, Trends Anal. Chem., 4, 5–6, 1985.
Hwang, I., Hopke, P. K., and Pinto, J. P.: Source apportionment and spatial distributions of coarse particles during the regional air pollution study, Environ. Sci. Technol., 42, 3524–3530, 2008.
Kim, S. W., Yoon, S. C., Won, J. G., and Choi, S. C.: Ground-based remote sensing measurements of aerosol and ozone in an urban area: a case study of mixing height evolution and its effects on ground-level ozone concentrations, Atmos. Environ., 41, 7069–7081, 2007.
Lagudu, D. R. K., Raja, S., Hopke, P. K., Chalupa, D. C., Utell, M. J., Casuccio, G., Lersch, T. L., and West, R. R.: Heterogeneity of coarse particles in an urban area, Environ. Sci. Technol., 45, 3188–3296, 2011.

ACPD
15, 14889–14921, 2015

Langford, A. O., Senff, C. J., Banta, R. M., Hardesty, R. M., Alvarez, R. J., Sandberg, Scott, P., and Darby, L., S.: Regional and local background ozone in Houston during Texas Air Quality Study, J. Geophys. Res., 114, D00F12, doi:10.1029/2008JD011687, 2009.
Lena, F. and Desiato, F.: Intercomparison of nocturnal mixing height estimate methods for urban air pollution modeling, Atmos. Environ., 33, 2385–2393, 1999.
Li, S. M.: A concerted effort to understand the ambient particulate matter in the Lower Fraser Valley: the Pacific 2001 Air Quality Study, Atmos. Environ., 38, 5719–5731, 2004.
Liu, P. F., Zhao, C. S., Göbel, T., Hallbauer, E., Nowak, A., Ran, L., Xu, W. Y., Deng, Z. Z., Ma, N., Mildenberger, K., Henning, S., Stratmann, F., and Wiedensohler, A.: Hygroscopic properties of aerosol particles at high relative humidity and their diurnal variations in the North China Plain, Atmos. Chem. Phys., 11, 3479–3494, doi:10.5194/acp-11-3479-2011, 2011.
Liu, W. X., Coveney, R. M., and Chen, J. L.: Environmental quality assessment on a river system polluted by mining activities, Appl. Geochem., 18, 749–764, 2003.
McKendry, I. G., Stahl, K., and Moore, R. D.: Synoptic sea-level pressure patterns generated by a general circulation model: comparison with types derived from NCEP/NCAR re-analysis and implications for downscaling, Int. J. Climatol., 26, 1727–1736, 2006.
Menichini, E., Iacovella, N., Monfredini, F., and Turrio-Baldassarri, T.: Atmospheric pollution by PAHs, PCDD/Fs and PCBs simultaneously collected at a regional background site in central Italy and at an urban site in Rome, Chemosphere, 69, 422–434, 2007.
Pérez, J., Pey, S., Castillo, M., and Viana, A.: Interpretation of the variability of levels of regional background aerosols in the western Mediterranean, Sci. Total Environ., 407, 527–540, 2008.
Ronald, C.: Gaseous contaminant filtration: keeping commercial buildings clean, Filtr. Separat., 44, 24–26, 2007.
Schwartz, S. E.: The white house effect – shortwave radiative forcing of climate by anthropogenic aerosols: an overview, J. Aerosol Sci., 27, 359–382, 1996.
Seibert, P., Beyrich, F., Gryning, S. E., Joffred, S., Rasmussene, A., and Tercierf, P.: Review and intercomparison of operational methods for the determination of the mixing height, Atmos. Environ., 34, 1001–1027, 2000.
Strader, R., Lurmann, F., and Pandis, S. N.: Evaluation of secondary organic aerosol formation in winter, Atmos. Environ., 33, 4849–4863, 1999.
Shi, G. L., Li, X., Feng, Y. C., Wang, Y. Q., Wu, J. H., Li, J., and Zhu, T.: Combined source apportionment, using positive matrix factorization–chemical mass balance and principal com-

ACPD
15, 14889–14921, 2015

ponent analysis/multiple linear regression-chemical mass balance models, Atmos. Environ., 43, 2929–2937, 2009.
Shi, G. L., Tian, Y. Z., Zhang, Y. F., Ye, W. Y., Li, X., Tie, X. X., Feng, Y. C., and Zhu, T.: Estimation of the concentrations of primary and secondary organic carbon in ambient particulate matter: application of the CMB-Iteration method, Atmos. Environ., 45, 5692–5698, 2011.
Tchepel, O., Costa, A. M., Martins, H., Ferreira, J., Monteiro, A., Miranda, A. I., and Borrego, C.: Determination of background concentrations for air quality models using spectral analysis and filtering of monitoring data, Atmos. Environ., 44, 106–114, 2010.
Tie, X. X., Brasseur, G. P., Zhao, C. S., Granierc, C., Massiea, S., Qin, Y., Wang, P. C., Wang, G., Yang, P. C., and Richter, A.: Chemical characterization of air pollution in eastern China and the eastern United States, Atmos. Environ., 40, 2607–2625, 2006.
Tian, Y. Z., Wu, J. H., Shi, G. L., Wu, J. Y., Zhang, Y. F., Zhou, L. D., Zhang, P., and Feng, Y. C.: Long-term variation of the levels, compositions and sources of size-resolved particulate matter in a megacity in China, Sci. Total Environ., 463, 462–468, 2013.
Torrence, C. and Compo, G. P.: A practical guide to wavelet analysis, B. Am. Meteor. Soc., 79, 61–78, 1998.
US Environmental Protection Agency (USEPA): EPA CMB8.2 User's Manual, Office of Air Quality Planning and Standards, Research Triangle Park, NC 27711, 2004.
Watson, J. G., Cooper, J. A., and Huntzicker, J. J.: The effective variance weighting for least squares calculations applied to the mass balance receptor model, Atmos. Environ., 18, 1347–1355, 1984.
Watson, J. G., Zhu, T., Chow, J. C., Engelbrecht, J., Fujita, E. M., and Wilson, W. E.: Receptor modeling application framework for particle source apportionment, Chemosphere, 49, 1093–1136, 2002.
Watson, J. G., Chen, L. W. A., Chow, J. C., Doraiswamy, P., and Lowenthal, D. H.: Source apportionment: findings from the U.S. Supersites Program, J. Air Waste Manage., 58, 265–288, 2008.
Wongphatarakul, V., Friedlander, S. K., and Pinto, J. P.: A comparative study of $PM_{2.5}$ ambient aerosol chemical databases, Environ. Sci. Technol., 32, 3926–3934, 1998.
World Health Organization (WHO): Glossary on Air Pollution, WHO Regional Publications, Eur. Series No. 9, Regional Office for Europe, Copenhagen, 1980.

ACPD
15, 14889–14921, 2015

Xiao, Z. M., Wu, J. H., Han, S. Q., Zhang, Y.F, Xu, H., Zhang, X. Y., Shi, G. L., and Feng, Y. C.: Vertical characteristics and Source identification of PM_{10} in Tianjin, J. Environ. Sci., 24, 12–115, 2012.

Zeng, Y. and Hopke, P. K.: A study of the sources of acid precipitation in Ontario, Canada, Atmos. Environ., 23, 1499–1509, 1989.

ACPD

15, 14889–14921, 2015

Table 1. Height-to-height correlation coefficient of PM_{10} concentration.

	10 m	40 m	120 m	220 m
10 m	1.0			
40 m	0.96	1.0		
120 m	0.91	0.94	1.0	
220 m	0.72	0.76	0.85	1.0

ACPD
15, 14889–14921, 2015

Table 2. Pair-wise CD values at different heights.

	10 m	40 m	120 m
40 m	0.10		
120 m	0.15	0.11	
220 m	0.33	0.30	0.59

ACPD
15, 14889–14921, 2015

Table 3. The concentration of chemical components of ambient PM_{10} at 4 height sampling sites ($\mu g\,m^{-3}$).

	10 m mean	SD	40 m mean	SD	120 m mean	SD	220 m mean	SD
Na	1.60	0.71	1.34	0.58	1.28	0.48	0.89	0.41
Mg	1.51	0.54	1.29	0.92	0.99	0.52	0.54	0.36
Al	6.3	2.5	5.9	2.1	4.9	1.7	4.0	1.7
Si	8.5	4.6	6.8	2.9	6.4	2.8	4.9	2.8
P	ND	ND	ND	ND	ND	ND	ND	ND
K	1.41	0.72	1.02	0.44	1.11	0.68	0.70	0.35
Ca	7.1	2.8	5.1	2.0	4.6	2.2	2.5	1.6
Ti	0.23	0.12	0.19	0.12	0.24	0.20	0.29	0.53
V	ND	ND	ND	ND	ND	ND	ND	ND
Cr	0.04	0.03	0.04	0.03	0.05	0.04	0.04	0.04
Mn	0.09	0.05	0.06	0.03	0.06	0.03	0.04	0.02
Fe	2.51	1.22	2.08	1.21	1.92	1.09	1.09	0.80
Ni	0.01	0.02	0.01	0.01	0.02	0.03	0.03	0.05
Co	0.01	ND	ND	ND	ND	ND	0.01	0.01
Cu	0.20	0.17	0.14	0.22	0.09	0.13	0.02	0.03
Zn	0.69	0.32	0.60	0.31	0.55	0.28	0.27	0.16
Br	ND	ND	ND	ND	ND	ND	ND	ND
Ba	ND	ND	ND	ND	ND	ND	ND	ND
Pb	0.06	0.06	0.06	0.06	0.05	0.05	0.03	0.03
OC^*	13.5	6.2	10.8	4.6	9.6	3.8	7.3	3.1
EC^*	7.0	2.2	5.3	2.0	4.4	1.8	3.0	1.6
NH_4^+	6.2	3.5	6.3	3.4	6.9	3.1	5.7	4.0
Cl^-	6.4	5.3	5.6	4.1	5.0	3.0	1.7	1.2
NO_3^-	18.0	12.5	16.9	10.9	18.9	10.1	13.3	11.4
SO_4^{2-}	27.4	20.6	26.1	17.5	25.3	16.4	19.7	16.2
OC/EC	1.91	2.79	2.03	2.26	2.20	2.10	2.40	1.90
PM_{10}	140	48	120	44	108	41	80	39

OC: organic carbon.
EC: element carbon.

ACPD
15, 14889–14921, 2015

Table 4. Source contributions and percentage contributions at four different heights.

		coal combustion	crustal dust	cement dust	vehicle exhaust	secondary sulfate	secondary nitrate	TOT
contribution ($\mu g\,m^3$)	10 m	17	16	14	20	34	23	140
	40 m	16	13	10	17	33	21	120
	120 m	14	12	8	15	32	24	108
	220 m	12	9	4	12	25	17	80
percentage (%)	10 m	12	11	10	14	24	16	88
	40 m	13	11	8	14	27	18	90
	120 m	13	11	8	14	29	22	97
	220 m	14	11	5	15	31	21	97

ACPD
15, 14889–14921, 2015

Table 5. Values of the parameters of the Morlet transform in this study.

C_δ	ψ_0	s_0	δt	δj	ω_0
0.776	$\pi^{-1/4}$	$2\delta t$	2	0.25	6.0

ACPD
15, 14889–14921, 2015

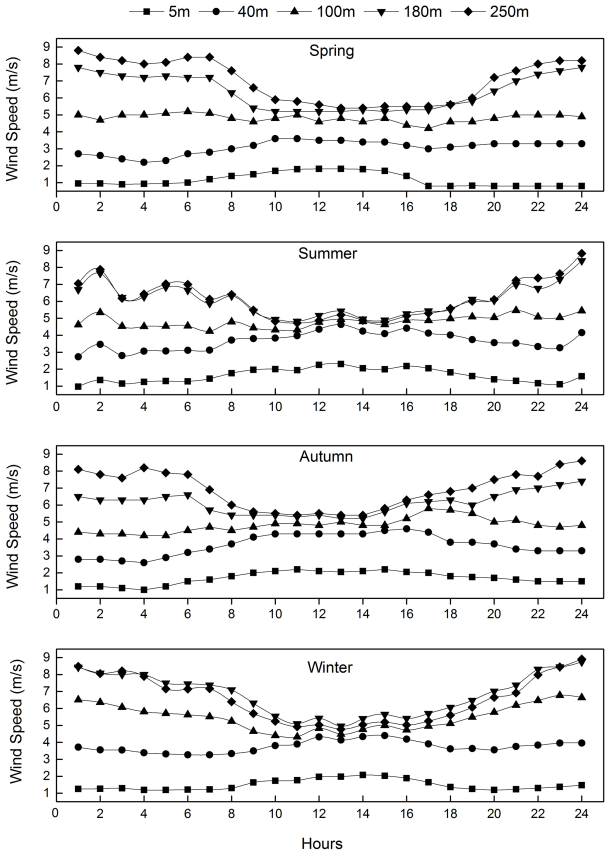

Figure 1. Diurnal variation of averaged wind speed in each season at different heights.

ACPD
15, 14889–14921, 2015

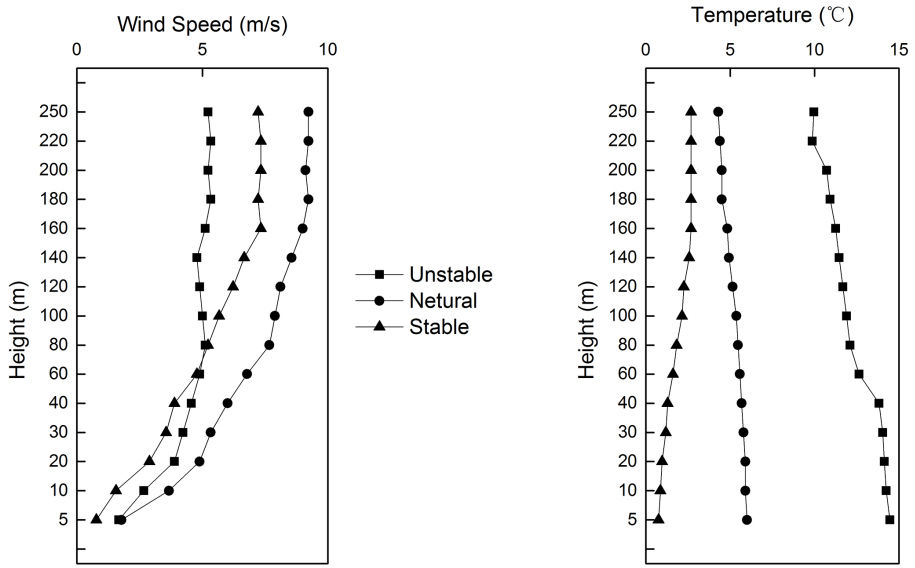

Figure 2. Vertical distribution profile of average wind speed and temperature under different stability.

ACPD
15, 14889–14921, 2015

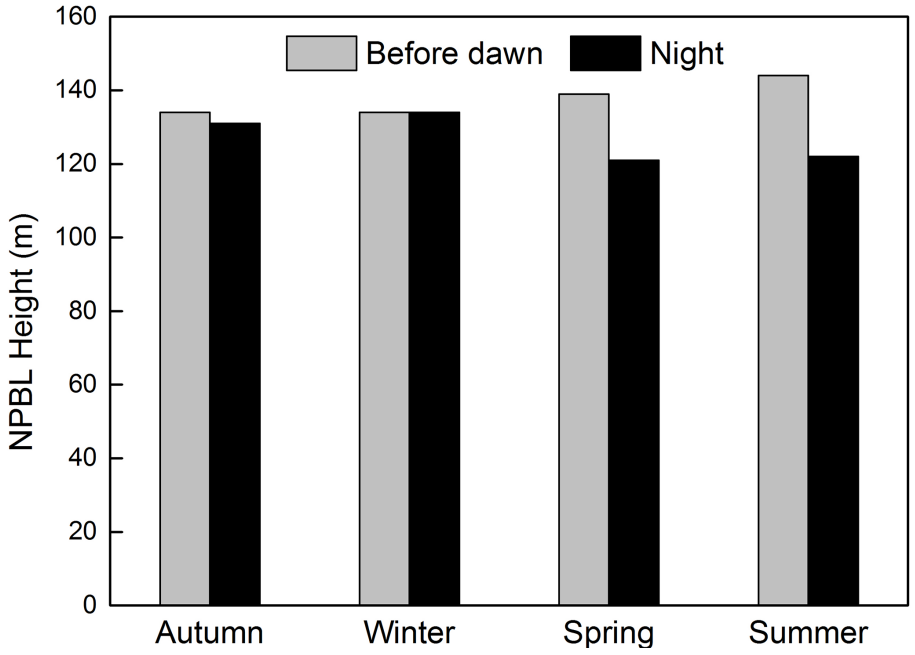

Figure 3. Averaged NPBL height in each season (before dawn: 01:00–07:00 LT; at night: 19:00–24:00 LT).

ACPD
15, 14889–14921, 2015

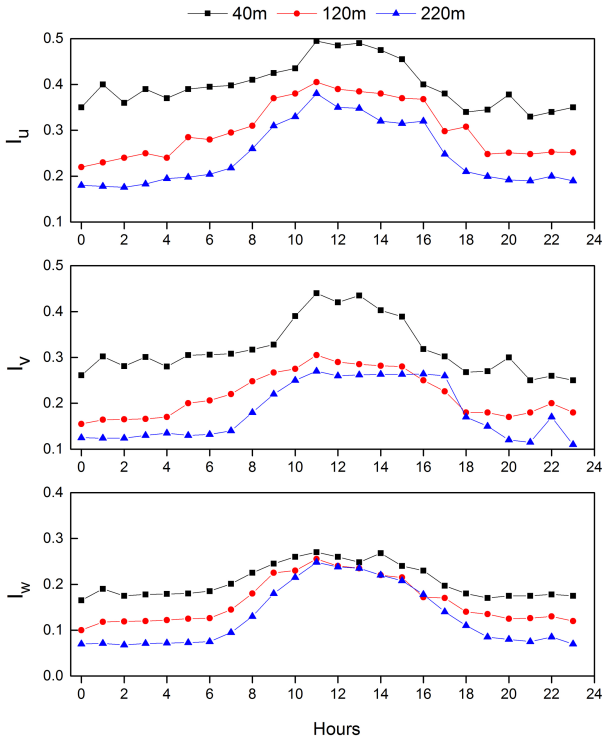

Figure 4. Averaged diurnal variation of three dimensional components of turbulent intensity at different heights (longitudinal turbulent intensity I_u, lateral turbulent intensity I_v,vertical turbulent intensity I_w).

ACPD
15, 14889–14921, 2015

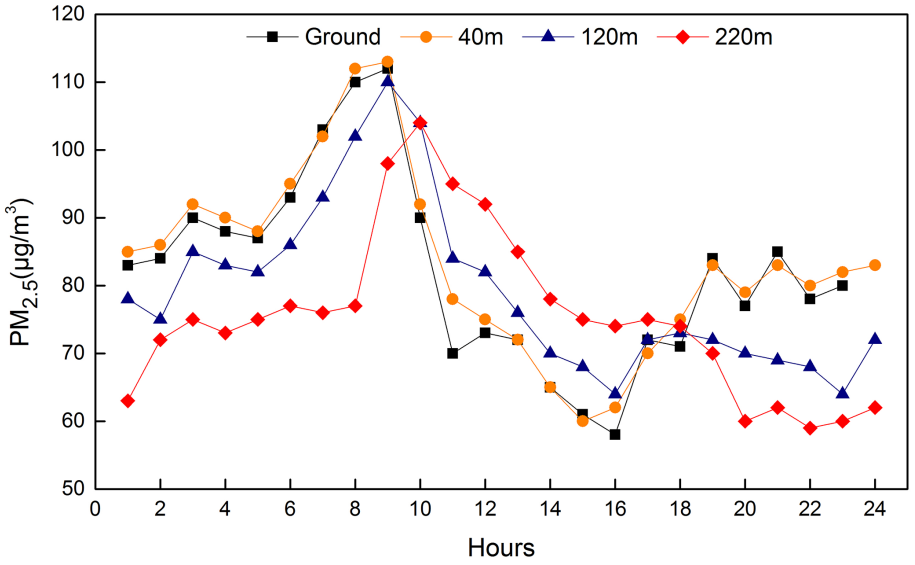

Figure 5. Vertical diurnal variation of $PM_{2.5}$ mass concentration in fall.

ACPD
15, 14889–14921, 2015

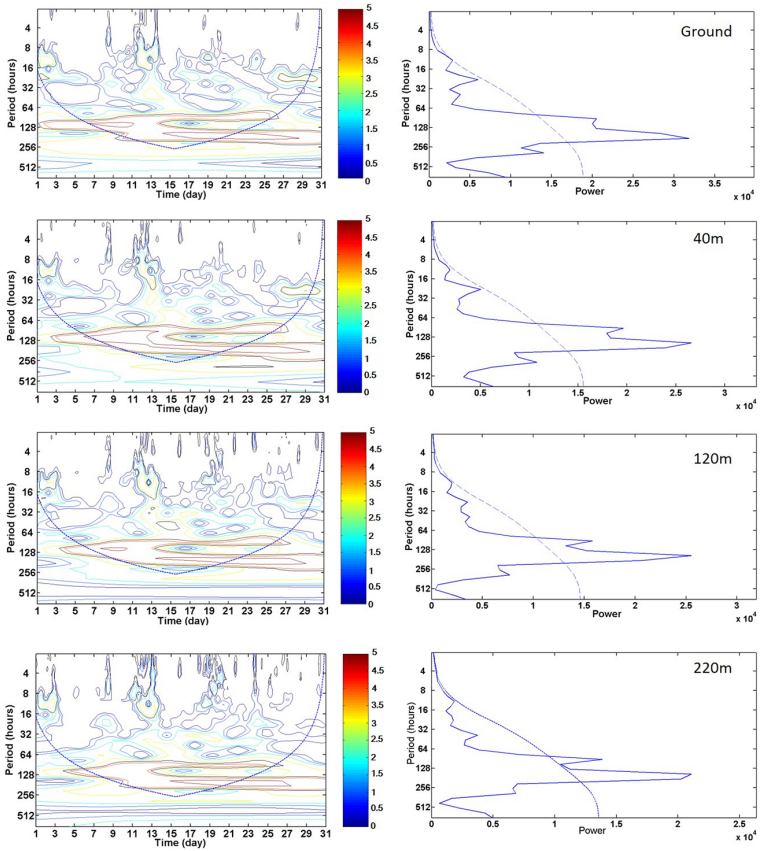

Figure 6. Local (left figure) and global (right figure) wavelet power spectrum of $PM_{2.5}$ mass concentration at different heights in August.

ACPD
15, 14889–14921, 2015

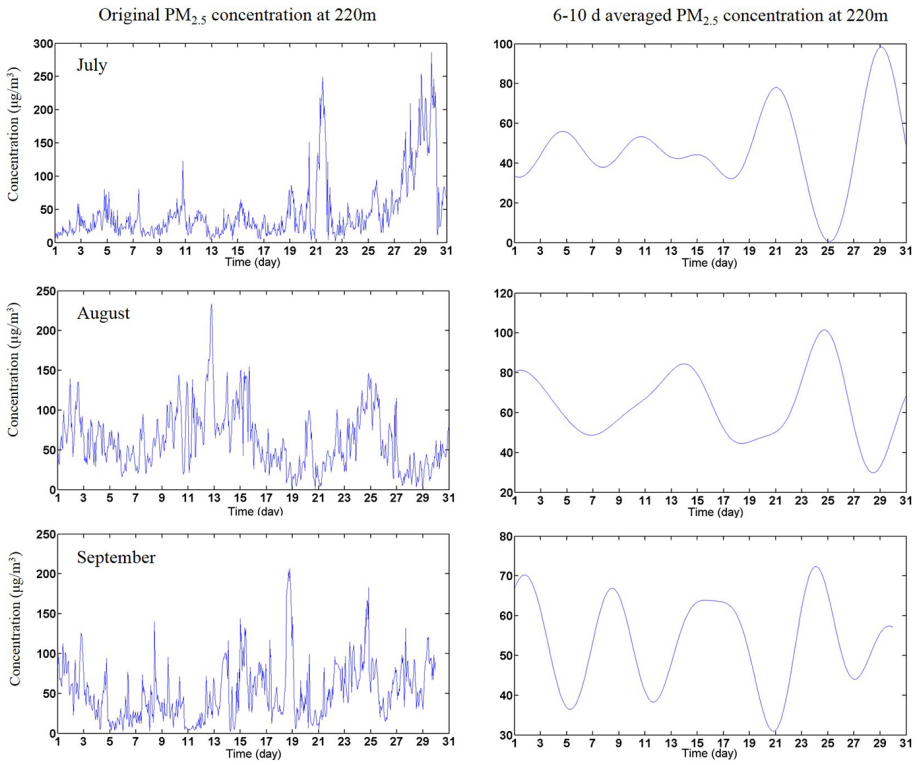

Figure 7. Time series of $PM_{2.5}$ hourly concentration before and after the filtering.

ACPD
15, 14889–14921, 2015